Toward a Deeper Understanding of Enzyme Reactions Using the Coupled ELF/NCI Analysis: Application to DNA Repair Enzymes

Dong Fang,[†] Robin Chaudret,[‡,§,∥] Jean-Philip Piquemal,*[,‡,§] and G. Andrés Cisneros*[,†]

[†]Department of Chemistry, Wayne State University, 5101 Cass Ave., Detroit, Michigan 48202, United States
[‡]UPMC Univ Paris 06, UMR 7616 Laboratoire de Chimie Théorique, Case Courrier 137, 4 Place Jussieu, F-75005, Paris, France
[§]CNRS, UMR 7616, Laboratoire de Chimie Théorique, Case Courrier 137, 4 Place Jussieu, F-75005, Paris, France

Ⓢ Supporting Information

ABSTRACT: The combined Electron Localization Funtion (ELF)/ Noncovalent Interaction (NCI) topological analysis (Gillet et al. *J. Chem. Theory Comput.* **2012**, *8*, 3993) has been extended to enzymatic reaction paths. We applied ELF/NCI to the reactions of DNA polymerase λ and the ε subunit of DNA polymerase III. ELF/NCI is shown to provide insights on the interactions during the evolution of enzymatic reactions including predicting the location of TS from structures located earlier along the reaction coordinate, differential metal coordination, and on barrier differences with two different cations.
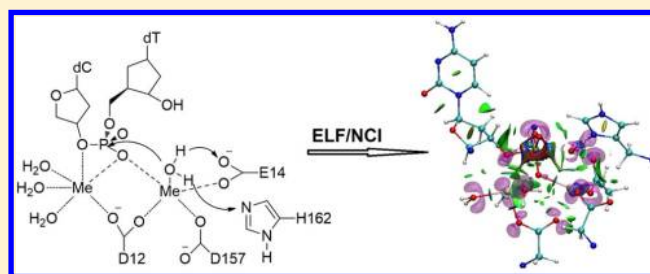
DNA polymerases and exonucleases play an important role in DNA replication and repair.[1,2] DNA polymerases catalyze the addition of incoming deoxyribonucleotides (dNTP) to a nascent DNA chain. According to the primary structure of their catalytic subunits, DNA polymerases are categorized into several different families.[3] Human DNA polymerase λ is a member of the X family and has been implicated in the gap filling and end joining processes involved in the repair of DNA double-strand breaks and in base excision repair of damaged bases.[4,5] Exonucleases catalyze the inverse reaction of polymerases, i.e., the excision of DNA bases. As a catalytic subunit of *E. coli* DNA polymerase III, subunit ε accounts for the proofreading exonuclease activity by catalyzing the removal of newly incorporated mispaired nucleotides.[6−8]

Recently, some of us introduced a coupling of two quantum interpretative techniques using both the Electron Localization Function (ELF)[9−11] and the Noncovalent Interaction (NCI)[12,13] index to study reaction mechanisms through a partition of the electronic density. This combined ELF/NCI analysis was initially applied to investigate in detail prototypical organic reactions[14] since this cross interpretative approach enables the following of the full range of interactions within a complex system. Indeed, ELF/NCI is able to simultaneously unravel regions of strong electron pairing (atoms and bonds) using ELF and regions of low density associated with low density reduced gradient, revealing weak interactions using NCI. This approach has been automated and gives chemically intuitive and visual results to describe chemical reactions involving multiple steps.[14] In this contribution, we propose the first application of this technique to large systems of biological interest using hybrid QM/MM (Quantum Mechanics/Molecular Mechanics) methods. To this end, we have applied ELF/ NCI analysis to study the reactions catalyzed by DNA polymerase λ (Polλ) and the ε subunit of PolIII (ε). The reaction paths associated with the catalytic mechanisms of these two enzymes have been studied in detail by some of us previously using QM/MM simulations.[15,16] In both cases, two divalent metal cations are required for catalysis. Both DNA polymerases and exonucleases can employ different metals for catalysis.[17−19] In our previous studies, we have investigated the role of Mg^{2+} and Mn^{2+} for the reaction mechanism catalyzed by both enzymes.[15,16] In addition, we have recently used ELF to investigate metal ion mutagenicity in the synthesis of DNA by Polλ.[17]

The ELF function was originally proposed to measure the electron localization in atomic and molecular systems based on the Hartree−Fock formalism[9] and subsequently extended to DFT.[20] Similarly to the Bader and Austen's topological analysis of the electron density,[21] the ELF values can also be treated as a continuous and differentiable scalar field in 3D space. The maxima of ELF (critical points) are named attractors and are located on atoms, bonds, and lone pairs following chemical intuition. Consequently, the molecular space can be divided into regions, named basins, that respectively contain all points whose ELF gradient field converges toward the same attractor. The different basins do not overlap, and the surface separating two basins is called a separatrix. Depending on the electrons they refer to, the different basins can be denoted as C() for core electrons or V() for valence electrons. Core basins are defined as belonging to a single nucleus. Valence basins may belong to a single atom and are termed monosynaptic (e.g., lone pairs) or
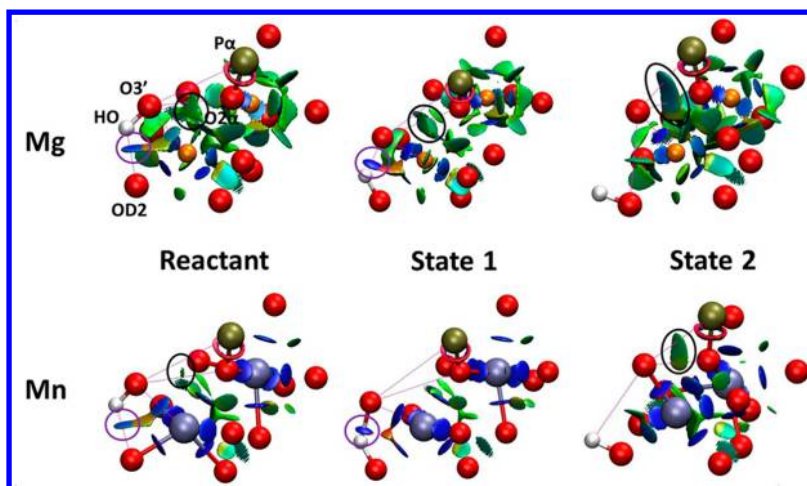
Figure 1. NCI analysis for the reactant, TS (state 1), and transphosphorilation structure (state 2) of Polλ with Mg^{2+} and Mn^{2+} (the isovalue is 0.4 au, and the color scale is −0.04 au < sign($\lambda2$)ρ < 0.04 au).

may belong to two (or three) atoms and are termed disynaptic (e.g., bonds).

Recently, a third category has been proposed; subvalence electrons have been proposed to be the outer-shell "core" electrons of specific metal cations.[18] Basins associated with chemical bonds between atoms X and Y are denoted as V(X,Y). Furthermore, the ability to divide the molecular space into regions allows not only the computation of integrated properties, such as charge and volume, but also local electrostatic multipoles or Fukui functions over these regions.[18,22]

The NCI[12,13] index enables the study of the domains of the electronic density associated with weak interactions that exhibit both low electron density <u>and</u> low reduced density gradient(s):

$$s(\rho) = \frac{|\nabla\rho|}{2(3\pi^2)^{1/3}\rho^{4/3}} \quad (1)$$

where ρ is the electron density. By multiplying the density by the sign of the second eigenvalue of the density Hessian (λ_2), one can distinguish the strength and the attractive or repulsive nature of the interactions.[23] In the noncovalent region, an arbitrary color code was chosen so that, for NCI surfaces: The red color is used for regions with a positive λ_2 that are associated with steric repulsion. The blue color is used for domains with a negative λ_2, therefore indicating relatively strong attraction (for example, H-bond regime). The green color is used for regions of very weak reduced density gradient, associated with van der Waals interactions. The ELF calculations were carried out using the TopMod software.[24] The NCI[12,13] results were calculated with the NCIPLOT program.[12,13] Details about the computations are available in the Supporting Information.

The ELF analysis of the critical structures for the reaction catalyzed by Polλ have been presented in a previous study.[17] Herein, only their NCI surfaces are discussed (the combined ELF/NCI surfaces are shown in Figure S1). The NCI analysis shows the evolution of the different interactions along the reaction path (see Figure 1). Interestingly, the interactions related to the two legs of the path are already visible at the reactant state. As expected, the strong interaction between HO and OD2 from Asp490 (circled in purple) clearly appears at the reactant state and evolves along the first part of the reaction (see reactant structure in Scheme 1 for atom labels). After the

Scheme 1. Reaction Mechanism for the Reaction Catalyzed by Polλ^a
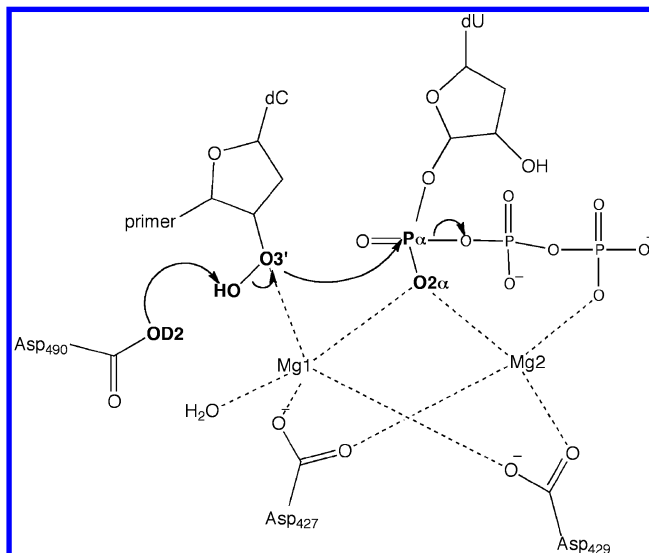
^{a}The atom labels used in the text are denoted in the reactant structure.

proton transfer, a strong hydrogen bond between O3′ and HO remains clearly visible. Concerning the second part of the reaction (transphosphorylation), the interaction between O3′ and O2α (circled in black), that can be seen from the reactant state, will evolve along the reaction path to give rise to the Pα–O3′ bond at the product state. The strength of this basin is characteristic of the van der Waals interactions at the reactant state; it will however evolve into a delocalized double basin whose attractive part is characteristic of the Pα–O3′ attraction and repulsive part of the O3′–O2α electrostatic repulsion. This is similar to the evolution of the C–C interaction into a C–C bond and the development of ring tension during the electrocyclization of butadiene as previously described.[14]

The comparison between the Mg^{2+} and Mn^{2+} NCI topologies shows some important differences. The O3′–Mg interaction is weaker than the O3′–Mn one. Conversely, the O3′–O2α interaction is weaker (and so is O$_3$′–Pα) in the Mn^{2+} structure than in the Mg^{2+} case. Indeed, since Mg^{2+} is a hard cation and Mn^{2+} is a soft one, the O3′–Mg interaction

involves less electrons than the O3′−Mn. Therefore, more electrons are accessible to the O−H bond and the other lone pair in the Mg case, suggesting that (i) the OD2−HO interaction is weaker because HO is less acidic and (ii) the O3′−O2α and Pα interaction is stronger. Finally, this is also consistent with our previous QM/MM energetic results that showed that the barrier for proton transfer is higher when Mg^{2+} is present in the active site compared to Mn^{2+}.[17]

As described above, ε catalyzes the excision of a nucleotide from DNA (see Scheme 2). Figure 2 shows the ELF and NCI

Scheme 2. Reaction Mechanism for the ε Subunit[a]
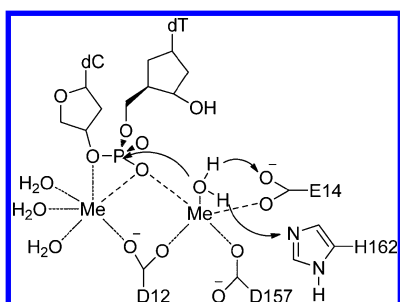
[a]In the first step, a proton is transferred from the ordered water to H162 to activate the nucleophile. Subsequently, the oxygen performs a nucleophilic attack to break the phosphoesther bond coupled with a second proton transfer to E14.[16]

surfaces of the critical points on the path for the reaction catalyzed by the ε subunit with Mg^{2+} and Mn^{2+}. As shown in Figure S2, the basins of the Mg^{2+} ions are spherical as expected. Conversely, there are several basins around each of the Mn^{2+}. This has been observed previously in the context of other metalloproteins and has been termed "subvalence splitting."[17,18] It has been shown that the splitting of the subvalence in metal

cations is due to the partial covalency between the metal cation and the ligands around it[18] and may be related to some biological features of the metal cations.[17,18]

Tables S1 and S2 (see Supporting Information) confirm the splitting of the electronic density of the two Mn^{2+}'s into several distinct basins, while that of the Mg^{2+} cations shows only one basin. This suggests that the interactions between the Mn^{2+} and the ligands in their first coordination shell are stronger than those of the Mg^{2+} and its corresponding ligands. For the Mn^{2+} cation, the catalytic metal (Me2, see Figure 3) has five
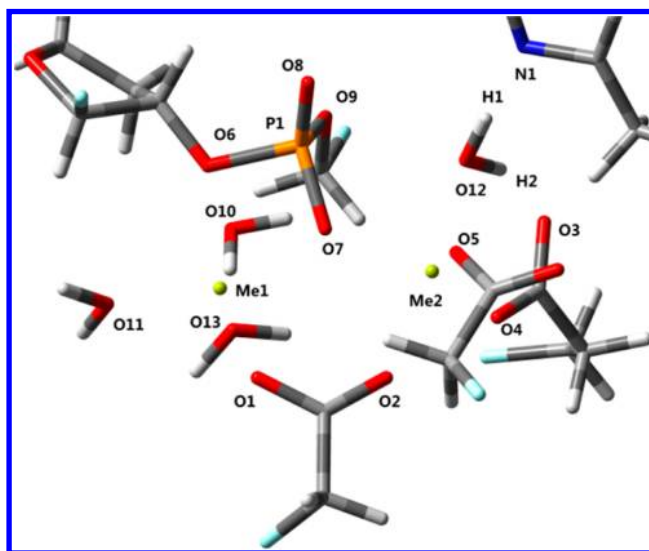
Figure 3. Numbering of the atoms in ε that are used in the ELF calculations.

subvalence basins while the binding metal (Me1) has six subvalence basins. In this special case, the number of the
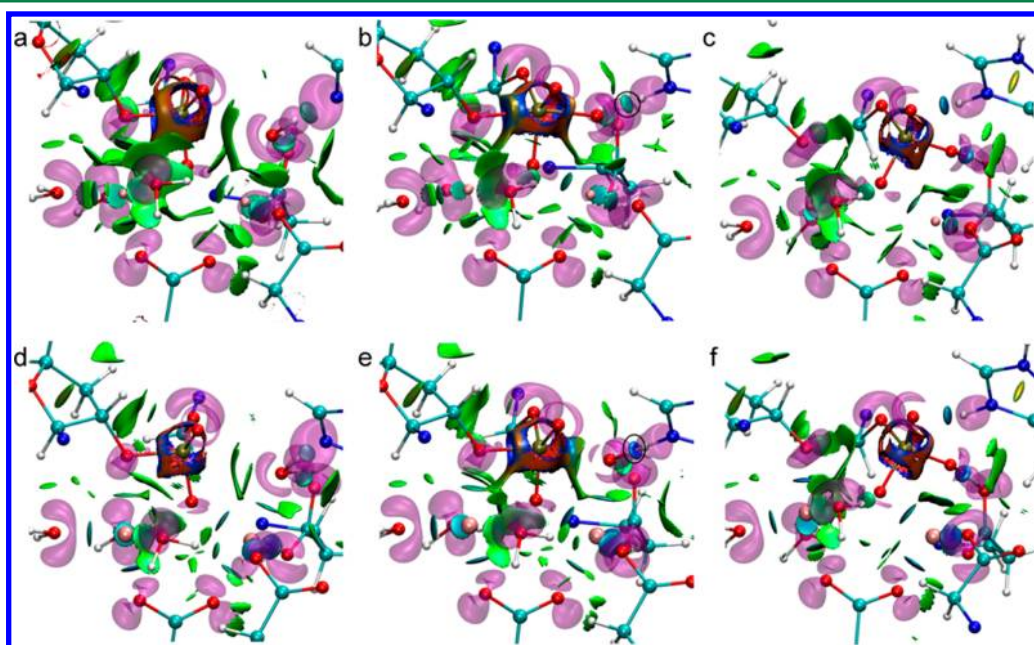
Figure 2. Combined ELF and NCI surfaces of the critical structures for the reaction catalyzed by the ε subunit with Mg^{2+} and Mn^{2+}. Only atoms subjected to the ELF analysis are shown; the rest of the QM subsystem is omitted for clarity. Panels a, b, and c show the reactant, TS, and product for Mg^{2+}, respectively. Panels d, e, and f correspond to the reactant, TS, and product for Mn^{2+}, respectively. The isovalue for ELF is 0.87, and for NCI it is 0.5 au with the color scale -0.1 au $<$ sign$(\lambda2)\rho < 0.1$ au.
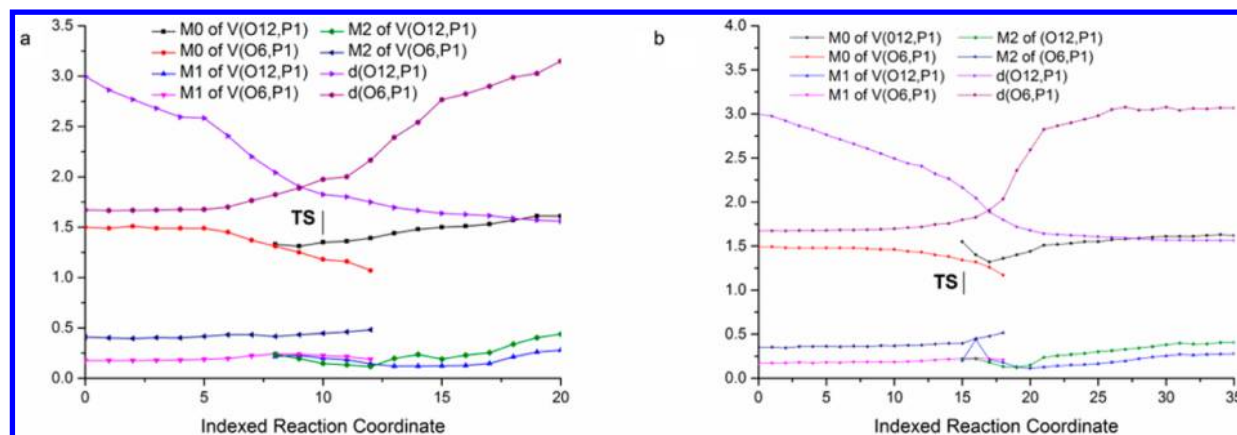
Figure 4. Distributed moments, M_0 (population), M_1 (first moment), and M_2 (second moment) of V(O6,P1) and V(O12,P1) and the distances (d(O6,P1) and d(O12,P1), in Å, along the reaction (a, b are for the reactions catalyzed by Mg^{2+} and Mn^{2+}, respectively).

splitting subvalence basins for each metal ion is equal to the number of ligands in the first coordination shell for Mn^{2+}. In addition, the number of basins in the subvalence for the metals remains constant during the progress of the reaction.

A multipolar expansion of the electron density of each ELF basin can provide further insight into the changes in the basins along the reaction thanks to the evaluation of local electrostatic moments. In this case, the first and second moments of each basin for both metal cations show only slight changes. However, ELF can also provide insights on the bonds that break (between O6 and P1) and form (between O12 and P1) during the reaction by analyzing the evolution of the basins associated with these bonds. Figure 4 shows the distance evolution O6−P1 and O12−P1 and the multipolar decomposition evolution (population, first and second moments, M_0, M_1, and M_2, respectively) of two bond basins, V(O6,P1) and V(O12,P1) for the Mn^{2+} and Mg^{2+} catalyzed reactions. In the case of the Mg^{2+} catalyzed reactions, the TS is late in the reaction coordinate, with a longer distance for the breaking bond, d(O6−P1), than for the forming bond, d(O12−P1). When Mn^{2+} is in the active site, the TS is located earlier in the path with a significantly shorter distance for the breaking bond and a longer distance for the forming bond. In particular, the two distances and the populations of these two basins change dramatically around the TS.

The most significant change is in the population of the basins for the forming and breaking bonds. Interestingly, the appearance of the V(O12,P1) basin (corresponding to the forming bond) shows significant differences between the two cations. In the case of Mg^{2+}, the basin appears before the system reaches the TS with a small population of 1.25, which increases continuously as the reaction reaches the TS and plateaus as the reaction continues to the product. For the Mn^{2+} case, the basin only arises at the TS with a much larger population of around 1.7, which shows a marked decrease and then an increase as the reaction proceeds. This population change indicates that the Mn^{2+} cation induces a larger charge transfer on the three atoms involved in these two basins. The earlier TS and larger population change in the Mn^{2+} catalyzed reaction help explain the lower energy barrier compared to the Mg^{2+} catalyzed reaction. The first and second moments (M_1 and M_2, respectively) for both basins show only modest variations along the path, indicating only a small change in polarization on these basins.

Since most of the time the interactions between the metal and its ligands are not traditional covalent bonding, no typical ELF basins for covalent bonds can be found. In this case, NCI plays an important role in the deep understanding of this type of intermolecular interaction. Indeed, the number of NCI surfaces is able to indicate the coordination number of Mg^{2+} and Mn^{2+} as well. For ε, the catalytic metal (Me2) is surrounded by five NCI surfaces for both cations, which suggests a penta-coordination in both cases. This is consistent with our previous results for the reaction path calculation, which showed that this penta-coordination on the catalytic metal polarizes the water to facilitate the first deprotonation.[16] In contrast, the nucleotide binding metal (Me1) is surrounded by six NCI surfaces for both Mg^{2+} and Mn^{2+}.

For the same metal center, different ligands produce NCI surfaces with different color depths, which can differentiate the strength of the interactions. Generally speaking, the NCI surfaces between ligands and the metal centers for Mn^{2+} are bluer than the ones in Mg^{2+}. This means that the interactions for Mn^{2+} are stronger than Mg^{2+}, which is in accord with the lower energy barrier for Mn^{2+}. For the metal in the reactant structure, the surfaces for O2, O7, O5, and O4 are bluer than the one for the oxygen of the nucleophilic water (O12). For Me1, O6 has the weakest interaction compared to the other ligands coordinated to Me1. Compared to the reactant, the surface between P1 and O12 in the TS becomes bluer, indicating the increasing attraction between these atoms as the bond forms. In addition, the blue surfaces between the transferred hydrogen atoms (H1, H2) show strong hydrogen bonding (circled in black, Figures 2b/e) with the corresponding oxygen atoms (O8, O12).

Thus, these two analyses are consistent with each other. Furthermore, regarding the proton H1, which is transferred from O12 to N1, in both TS structures it shows a shared basin with the lone electron pair of N1, which means the proton transfer from the nucleophilic water to N1 has already started. The distance between H1 and N1 is 1.06 Å for the Mg^{2+} catalyzed structure. For Mn^{2+}, the distance is 1.14 Å, close to the value for Mg^{2+}. However, for Mg^{2+}, the population of this shared basin is about 2.72. In comparison, for Mn^{2+}, H1 forms a "bond-like" basin with N with a population of 0.86. The rest of the lone pair of N1 forms an extra basin with a population that is 1.07. The NCI surfaces between H1 and O12 (circled in black in Figure 2) are much bluer for Mn^{2+} than for Mg^{2+}, indicating a stronger interaction between these atoms for Mn^{2+}

than for Mg^{2+}. This is in good agreement with the smaller basin population for the Mn^{2+} structure.

In general, in terms of NCI surfaces, Mn^{2+} cations have bluer NCI surfaces between the ligands than their corresponding Mg^{2+} cations. With regards to ELF, Mn^{2+} possesses more splitting basins. Both of them are suggestive of the stronger ligand interactions for Mn^{2+}, which is in agreement with its lower reaction barrier than Mg^{2+}.[15,16]

As shown in the movie in the Supporting Information, the NCI surfaces are able to help predict the forthcoming forming or breaking of bonds, and the ELF basins provide the details of existing bonds. When the bonds (for example, the bonds between O12 and P1, H1 and N1, and H2 and O3) begin to form as the reaction progresses, NCI surfaces appear and become bluer; then they turn into rings (due to the cutoff for the electron density, see Supporting Information) and enlarge gradually, concurrent with the appearance of ELF basins. When the bonds begin to break (for instance, O6−P1 and H1−O12), the ELF basins become smaller, coupled to the emergence of NCI surfaces. Similarly to the findings of Gillet et al.,[14] the ELF attractors and the NCI interaction critical points (the holes) overlap. That is, ELF basins appear where NCI surfaces disappear, and vice versa providing ways to anticipate transition states.

In summary, we have demonstrated the applicability of the recently developed ELF/NCI topological approach to complex enzyme reactions involving large biological systems treated at the QM/MM level. Once again, ELF and NCI have been found to be highly complementary, giving information on bond formation and breaking, and on weak interactions thanks to NCI, and on the reorganization of existing bonds and lone pairs with ELF. In addition, NCI was shown to be able to provide further insights into the factors governing the lowering of the reaction barrier in Polλ when Mn^{2+} is in the active site compared to Mg^{2+}. In the case of the ε subunit, both ELF and NCI proved to be useful in understanding the reasons for the lower barrier in the Mn^{2+} catalyzed reaction compared to Mg^{2+}. Moreover, the NCI analysis provided further support for the unusual penta-coordination observed in ε for the cation in the metal 2 position, which enables the activation of the nucleophile. Thus, the combination of these two techniques can be a useful and powerful tool to study the interaction changes along the enzyme reactions involved with metals. Finally, extending on the findings of Gillet et al.,[14] the ELF attractors and the NCI interaction critical points overlap as NCI critical points appear to be precursors of ELF attractors, providing new strategies to understand and predict the location of transition states in enzymes.

ASSOCIATED CONTENT

Ⓢ Supporting Information

Expanded computational details, combined ELF/NCI surfaces for Polλ structures, ELF basins of the metals, and animations of the evolution of ELF and NCI surfaces along the reaction path for reactions catalyzed by the ε subunit. This information is available free of charge via the Internet at http://pubs.acs.org/.

AUTHOR INFORMATION

Corresponding Author

*E-mail: jpp@lct.jussieu.fr (J.P.P.), andres@chem.wayne.edu (G.A.C.).

Present Address

‖IFP Energies Nouvelles, 1&4, Avenue des Bios-Préau, 92852 Rueil-Malmaison Cedex, France

Notes

The authors declare no competing financial interest.

REFERENCES

(1) Loeb, L. A.; Monnat, R. J. *Nat. Rev. Genet.* **2008**, *9*, 594−604.
(2) Thomas, K. R.; Olivera, B. M. *J. Biol. Chem.* **1978**, *253*, 424−429.
(3) Bebenek, K.; Kunkel, T. A. *Adv. Protein Chem.* **2004**, *69*, 137−165.
(4) Garcia-Diaz, M.; Bebenek, K.; Gao, G.; Pedersen, L. C.; London, R. E.; Kunkel, T. A. *DNA Repair* **2005**, *4*, 1358−1367.
(5) Garcia-Diaz, M.; Bebenek, K.; Krahn, J. M.; Pedersen, L. C.; Kunkel, T. A. *Cell* **2006**, *124*, 331−342.
(6) Brenowitz, S.; Kwack, S.; Goodman, M. F.; O'Donnell, M.; Echols, H. *J. Biol. Chem.* **1991**, *266*, 7888−7892.
(7) McHenry, C. S. *J. Biol. Chem.* **1991**, *266*, 19127−19130.
(8) Derbyshire, V.; Pinsonneault, J. K.; Joyce, C. M. *Methods Enzymol.* **1995**, *262*, 363−385.
(9) Becke, A. D.; Edgecombe, K. E. *J. Chem. Phys.* **1990**, *92*, 5397−5403.
(10) Piquemal, J. P.; Pilmé, J.; Parisel, O.; Gérard, H.; Fourré, I.; Bergès, J.; Gourlaouen, C.; De La Lande, A.; Van Severen, M. C.; Silvi, B. *Int. J. Quantum Chem.* **2008**, *108*, 1951−1969.
(11) Silvi, B.; Savin, A. *Nature* **1994**, *371*, 683−686.
(12) Contreras-García, J.; Johnson, E. R.; Keinan, S.; Chaudret, R.; Piquemal, J.-P.; Beratan, D. N.; Yang, W. *J. Chem. Theory Comput.* **2011**, *7*, 625−632.
(13) Johnson, E. R.; Keinan, S.; Mori-Sánchez, P.; Contreras-García, J.; Cohen, A. J.; Yang, W. *J. Am. Chem. Soc.* **2010**, *132*, 6498−6506.
(14) Gillet, N.; Chaudret, R.; Contreras-García, J.; Yang, W.; Silvi, B.; Piquemal, J.-P. *J. Chem. Theory Comput.* **2012**, *8*, 3993−3997.
(15) Cisneros, G. A.; Perera, L.; García-Díaz, M.; Bebenek, K.; Kunkel, T. A.; Pedersen, L. G. *DNA Repair* **2008**, *7*, 1824−1834.
(16) Cisneros, G. A.; Perera, L.; Schaaper, R. M.; Pedersen, L. C.; London, R. E.; Pedersen, L. G.; Darden, T. A. *J. Am. Chem. Soc.* **2009**, *131*, 1550−1556.
(17) Chaudret, R.; Piquemal, J.-P.; Cisneros, G. A. *Phys. Chem. Chem. Phys.* **2011**, *13*, 11239−11247.
(18) de Courcy, B.; Pedersen, L. G.; Parisel, O.; Gresh, N.; Silvi, B.; Pilmé, J.; Piquemal, J. P. *J. Chem. Theory Comput.* **2010**, *6*, 1048−1063.
(19) Sirover, M. A.; Loeb, L. A. *Science* **1976**, *194*, 1434−1436.
(20) Savin, A.; Jepsen, O.; Flad, J.; Andersen, O.; Preuss, H.; von Schnering, H. *Angew. Chem., Int. Ed.* **1992**, *31*, 187−188.
(21) Bader, R. F. W.; Austen, M. A. *J. Chem. Phys.* **1997**, *107*, 4271−4285.
(22) Pilmé, J.; Piquemal, J.-P. *J. Comput. Chem.* **2008**, *29*, 1440−1449.
(23) Contreras-Garcia, J.; Yang, W.; Johnson, E. R. *J. Phys. Chem. A* **2011**, *115*, 12983−12990.
(24) Noury, S.; Krokidis, X.; Fuster, F.; Silvi, B. *Comput. Chem.* **1999**, *23*, 597−604.